Journal of Biomedical Optics

SPIEDigitalLibrary.org/jbo

# Monte Carlo modeling of *in vivo* protoporphyrin IX fluorescence and singlet oxygen production during photodynamic therapy for patients presenting with superficial basal cell carcinomas

Ronan M. Valentine
C. Tom A. Brown
Harry Moseley
Sally Ibbotson
Kenny Wood

SPIE

# Monte Carlo modeling of *in vivo* protoporphyrin IX fluorescence and singlet oxygen production during photodynamic therapy for patients presenting with superficial basal cell carcinomas

**Ronan M. Valentine,[a,b] C. Tom A. Brown,[a] Harry Moseley,[b] Sally Ibbotson,[b] and Kenny Wood[a]**
[a]University of St. Andrews, School of Physics and Astronomy, North Haugh, St. Andrews, Fife KY16 9SS, United Kingdom
[b]University of Dundee, The Photobiology Unit, Ninewells Hospital & Medical School, Dundee DD1 9SY, United Kingdom

**Abstract.** We present protoporphyrin IX (PpIX) fluorescence measurements acquired from patients presenting with superficial basal cell carcinoma during photodynamic therapy (PDT) treatment, facilitating *in vivo* photobleaching to be monitored. Monte Carlo (MC) simulations, taking into account photobleaching, are performed on a three-dimensional cube grid, which represents the treatment geometry. Consequently, it is possible to determine the spatial and temporal changes to the origin of collected fluorescence and generated singlet oxygen. From our clinical results, an *in vivo* photobleaching dose constant, $\beta$ of 5-aminolaevulinic acid–induced PpIX fluorescence is found to be $14 \pm 1$ J/cm$^2$. Results from our MC simulations suggest that an increase from our typical administered treatment light dose of 75–150 J/cm$^2$ could increase the effective PDT treatment initially achieved at a depth of 2.7–3.3 mm in the tumor, respectively. Moreover, this increase reduces the surface PpIX fluorescence from 0.00012 to 0.000003 of the maximum value recorded before treatment. The recommendation of administrating a larger light dose, which advocates an increase in the treatment time after surface PpIX fluorescence has diminished, remains valid for different sets of optical properties and therefore should have a beneficial outcome on the total treatment effect.  [DOI: 10.1117/1.3562540]

Keywords: protoporphyrin IX fluorescence; photodynamic therapy; photobleaching; singlet oxygen; photodynamic doses; superficial basal cell carcinoma; Monte Carlo simulations.

Paper 10264RR received May 17, 2010; revised manuscript received Jan. 21, 2011; accepted for publication Feb. 10, 2011; published online Apr. 4, 2011.

## 1 Introduction

Photodynamic therapy (PDT) is a multimodality cancer treatment available for the palliation or eradication of systemic and cutaneous malignancies. The administration of a photosensitizer followed by the irradiation of the target region of interest with light of an appropriate wavelength activates the photosensitiser.[1] The interaction between the excited photosensitizer and molecular oxygen can lead to the direct or indirect production of cytotoxic species such as radicals and singlet oxygen.[2] Singlet oxygen is believed to be the main cytotoxic agent involved in PDT in clinical practice.[3] PDT has been recognized as an effective treatment of nonmelanoma skin cancers (NMSCs);[4] however, further optimization for PDT treatment is required.

In the context of the clinical administration of PDT for dermatological conditions, the following quantities can be observed; the administered quantity of the exogenous photosensitizer prodrug, the time delay between this prodrug application and the onset of treatment, the wavelength of the incident light, and the light dose (in Joules per centimeters squared), which is used to describe light delivery during PDT and defined as the skin surface irradiance (in milliwatts per centimeters squared) multiplied by the treatment time (in seconds).[5]

The work of Wilson et al.[6] has shown that by employing a technique such as implicit dosimetry, fluorescence photobleaching may be used as a dose metric. Photobleaching may be described as the reduction in optical absorbance and/or fluorescence as the photosensitizer is photochemically destroyed by light.[6] Fluorescence and photobleaching measurements can contribute significantly to the development of photodynamic therapy dosimetry.[7,8] Robinson et al.[9] have suggested that a reduction in photosensitizer fluorescence caused by photobleaching is indicative of the photodynamic dose (PD) administered. It is therefore possible to monitor, via photosensitizer fluorescence measurements, the amount of drug in the tissue that has photobleached during PDT and relate it to the PD.[10]

Optical fluorescence spectroscopy offers rapid diagnostic information by using light-tissue interactions.[11] It is used for the early detection of cancerous and precancerous lesions and monitoring of PDT treatments. The interactions of light with biological tissue causes light absorption and scattering as the photons propagate through the tissue. The light-tissue interactions of absorption are attributed to melanin and hemoglobin concentration, while lipids and collagen are responsible for optical scattering in the tissue.[12]

Address all correspondence to: Ronan M. Valentine, University of St. Andrews, School of Physics and Astronomy, North Haugh, St. Andrews, Fife KY16 9SS, United Kingdom. Tel: +44(0) 7522 685108; E-mail: rmv3@st-andrews.ac.uk

1083-3668/2011/16(4)/048002/11/$25.00 © 2011 SPIE

In order to fully optimize clinical PDT treatments, new approaches must be taken to model the process, which, as well as taking into account the photochemical behavior discussed above, also take into account the propagation of both the treatment wavelengths and the subsequent fluorescence wavelengths used for monitoring within tissue. One approach is to use radiation transfer simulations. Monte Carlo (MC) radiation transfer (MCRT) modeling is a technique that solves the transfer equation using the probabilistic nature of photon interactions and has been used to simulate many such interactions, which have previously been modeled by several approximations, including the seven flux model[13] and the diffusion approximation.[14] It may be efficiently implemented without approximating the angular distribution of light, tissue geometry, and optical properties.[15] Furthermore, the MC technique provides accurate results for highly absorbing media at positions close to the surface and can handle the highly forward directed light-scattering characteristics of tissue.[12,16]

In this study, *in vivo* 5-aminolaevulinic acid (5-ALA)–induced PpIX fluorescence measurements have been recorded during clinical topical photodynamic therapy (T-PDT) in humans from the surface of superficial Basal Cell Carcinomas (sBCC). Using this diagnostic, a photobleaching dose constant, $\beta$, of 5-ALA-induced PpIX fluorescence was obtained for patients presenting with sBCC. These results were then incorporated into a three-dimensional (3-D) MC model that enabled predictions to be made about the efficacy of treatment in PDT. In particular, we have used our model to address the important question of how long after surface PpIX fluorescence has diminished the PDT treatment is still effective and to what depths below the surface is effective treatment provided. To more accurately represent clinical T-PDT, in this paper we consider a model with a tumor of finite size embedded and surrounded in normal tissue and subjected to a finite uniform superficial irradiation. To the best of our knowledge, we believe that this is the first time that data obtained directly from clinical PDT treatments has been combined with a 3-D MC model to enable modeling of a fully 3-D tumor phantom of finite size embedded in normal tissue.

## 2 Materials and Methods

### 2.1 *Clinical Topical Photodynamic Therapy Treatment*

PDT treatments were carried out at Ninewells Hospital and Medical School in Dundee, Scotland, United Kingdom, using the photosensitizer prodrug, 5-ALA. Formal consent was obtained from the patients before the study was undertaken. T-PDT was preformed using either of two light-emitting diode (LED) light sources, Aktilite CL16 and CL128 (PhotoCure ASA, Oslo, Norway). These commercial devices have identical spectra, where the peak irradiance occurs at a wavelength of 632 nm with a full width at half maximum of 19 nm. Both light sources were calibrated and traceable to national measurement standards.[17] Typical treatment times and skin surface irradiances are in the region of 15 min and 80 mW/cm$^2$, respectively. At our centre, a total treatment light dose (LD) of 75 J/cm$^2$ is administered during T-PDT. 5-ALA was topically applied to the lesional area. Following a 6-h incubation period; one skin lesion per patient was treated.

### 2.2 *Clinical Fluorescence Measurements from Superficial Basal Cell Carcinomas*

PpIX is naturally occurring and present in small quantities in cells. Uptake and conversion of 5-ALA to PpIX in diseased tissue leads to increased levels of PpIX in lesions. When PpIX is excited with light at a wavelength of ~405 nm, characteristic fluorescence is induced with a readily observable peak at ~635 nm. A high fluorescence ratio of tumor to surrounding tissue allows for demarcation of the tumor. In our study, fluorescence spectra were acquired using a custom-built optical biopsy system (University of Glasgow, Glasgow, United Kingdom) formed by a fiber-coupled fluorescence spectroscopy system.[18] The output from an LED emitting at 405 nm was coupled to a 400 $\mu$m core optical fiber probe used for both excitation and collection of fluorescent emission. PpIX fluorescence was induced in the skin, and spectra were recorded by placing the probe perpendicularly in contact with the tissue. From each individual lesion, eight fluorescence spectra were recorded before 5-ALA application, immediately before treatment, approximately halfway through treatment, and immediately after treatment. The mean spectrum was then calculated from each set of eight spectra for each lesion. Treatment was stopped briefly for ~1 min to allow for the halfway measurements to be carried out. All measurements were performed in a darkened room to minimize artifacts from ambient room light.

### 2.3 *Description and Validation of the Monte Carlo Radiation Transfer Code*

A fixed weight MCRT code was written and developed in FORTRAN 77 to simulate the scattering, absorption, fluorescence, and photobleaching processes present in T-PDT. It was possible to account for the generation and propagation of excitation photons, and of fluorescence photons emanating from a tumor embedded in normal skin tissue. We have also incorporated an algorithm in the code to determine the production of singlet oxygen in the tumor. Although other MC simulations of photon transport and fluorescence have been performed in multilayered tissues,[19,20] our 3-D MC code can calculate light distributions for a clinical T-PDT geometry where a tumor is embedded in normal skin tissue. Earlier studies have used this type of geometry to model the distribution of light within a tumor.[21,22] Our code, however, also incorporates different optical properties for normal and tumor tissue and the addition of a photosensitizer, namely, PpIX into the tumor. Furthermore, photobleaching has also been included. This enables the efficacy of T-PDT to be investigated.

Within our code, $\mu_a$ and $\mu_s$ are the tissue-absorption and -scattering coefficients, which can be varied depending on the depth within our phantom, and $g$ is the scattering anisotropy factor. The Henyey–Greenstein phase function[23] is adopted to approximate scattering in tissue and is mathematically expressed in the form

$$P(\theta) = \frac{1}{4\pi} \frac{1 - g^2}{[1 + g^2 - 2g\cos(\theta)]^{3/2}}, \quad (1)$$

where $P(\theta)$ is a probability density function and $\theta$ is the scattering angle in radians, which the photon is scattered through with

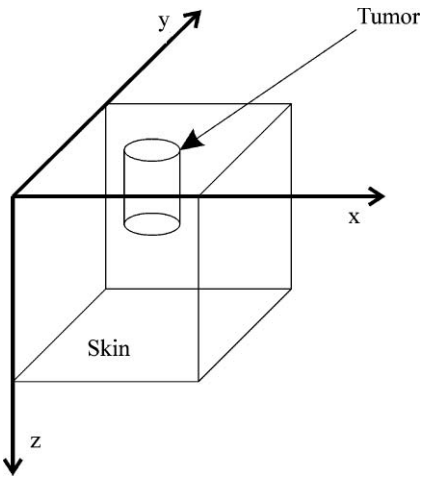


**Fig. 1** Three-dimensional (3-D) Monte Carlo model geometry, where *x, y* are mutually orthogonal axes in the skin surface and *z* represents depth within the skin tissue.

respect to the incident direction. $g$ is defined as

$$g \equiv \langle \cos(\theta) \rangle = \int_0^{\pi} p(\theta) \cos(\theta) 2\pi \sin\theta d\theta, \tag{2}$$

where

$$\int_0^{\pi} p(\theta) 2\pi \sin\theta d\theta = 1$$

$g$ affects the angular distribution and, therefore, the amount of forward direction maintained by the photon. At each interaction site, the probability of a photon being scattered or absorbed was determined by the albedo $a$, where a larger value of $a$ corresponds to a more highly scattering environment. Our model is based on a 3-D cube-shaped geometry[24–26] and removes the assumption of an optically semi-infinite tissue volume. To achieve statistical significance, simulations were performed with $10^8$ photons, on a 3-D Cartesian-grid geometry, as illustrated in Fig. 1. The tumor was placed at the surface of the skin. The total dimensions of the cube were taken to be $20 \times 20 \times 20$ mm $(x, y, z)$, and the modeled tumor had a radius of 5 mm and penetrated 4 mm into the cube. In our simplified situation, the tumor was represented by a cylinder and placed at the center of the normal skin tissue, which was represented by a cube. Our 3-D representation provides a reasonably accurate analog to the situation present in clinical T-PDT, where both the tumor and some of the surrounding normal skin tissue are superficially irradiated by a finite beam.

The Monte Carlo code was validated by comparing a range of simulations to the results generated by Keijzer et al.,[16] where light distributions in artery tissue were examined. For example, using a collimated incident-beam diameter of 1 mm, the fluence rates recorded from our simulations at the surface and at a depth of 0.5 and 1 mm into the tissue were 1.8, 0.55, and 0.11 W/cm$^2$, respectively. These results are comparable to those obtained by Keijzer et al.[16]

## 2.4 *Monte Carlo Model Assumptions*

With clinical T-PDT in mind, it was necessary to make some assumptions in our model. We have assumed mismatched boundary conditions, and in a similar method to Farrell et al.,[10] that the tumor had a homogeneous distribution of PpIX. The fluence rate distribution decays with tissue depth. Photobleaching alters the spatial distribution of PpIX in the tissue. The top layers experience the highest fluence rate and therefore photobleach faster.[10] We have assumed that the PpIX concentration has a negligible effect on the absorption coefficient of the tissue, therefore, resulting in a time-independent fluence-rate distribution.[27] PpIX photobleaching was assumed to follow a first-order exponential decay,[27] where the PpIX concentration, $C(x, y, z, t)$ decreased at a rate proportional to the local fluence rate, $\Psi(x, y, z)$, as is shown in

$$\frac{dC(x, y, z, t)}{dt} = -\frac{\Psi(x, y, z)}{\beta} C(x, y, z, t), \tag{3}$$

where $\beta$ is the photobleaching dose constant (in Joules per centimeters squared), $z$ represents the depth into the tissue, and $t$ s the treatment time point.

The dosimetric parameter, namely, the PD, is defined as the number of photons absorbed by the photosensitizer per unit volume of tumor tissue and is assumed to be proportional to the local yield of singlet oxygen production.[10] A threshold photodynamic dose ($PD_T$), leads to tissue necrosis if the number of photons absorbed by the photosensitizer per unit volume of tumor tissue exceeds a certain value. A threshold value of approximately $8.6 \times 10^{17}$ photons/cm$^3$ absorbed by a porphyrin photosensitizer in tumors was used.[28] Again, following the work of Farrell et al.,[10] we assumed that the local yield of singlet oxygen production following absorption by the photosensitizer defined the PD and tissue necrosis was assumed to occur when $PD > PD_T$. The PD is directly related to the photosensitizer concentration and the light fluence rate, as is shown in

$$\frac{d\mathrm{PD}}{dt} = \gamma_0 \Psi(x, y, z) C(x.y.z, t), \tag{4}$$

where $\gamma_0$ is the constant quantum yield for singlet oxygen production when the photodynamic therapy process was not limited by the availability of oxygen concentration.[10]

## 2.5 *Application of the Monte Carlo Model to Clinical Photodynamic Therapy*

On the basis of our assumptions, we modeled a clinical situation, i.e., the treatment itself and the fluorescence measurements undertaken during treatment requiring two different sets of simulations to be undertaken. The former consisted of simulations where the singlet oxygen produced in the tumor was modeled as a function of depth and time, whereas the latter included modeling the PpIX fluorescence detected at particular time points in the treatment. In this way, our model could provide information about both the fluorescence information used as a diagnostic and the possibility of tumor cell kill. We sampled the fluorescence emission in the code from clinically measured 5-ALA-induced PpIX fluorescence spectral data. This approach is different from other models, where only excitation and fluorescence emission wavelengths have been used rather than full spectral data.[27,29] Figure 2 depicts the optical properties used in the Monte Carlo simulations, which were taken from data published in the literature.[30–32] Figure 3 illustrates our absorption coefficient for PpIX as a function of wavelength.

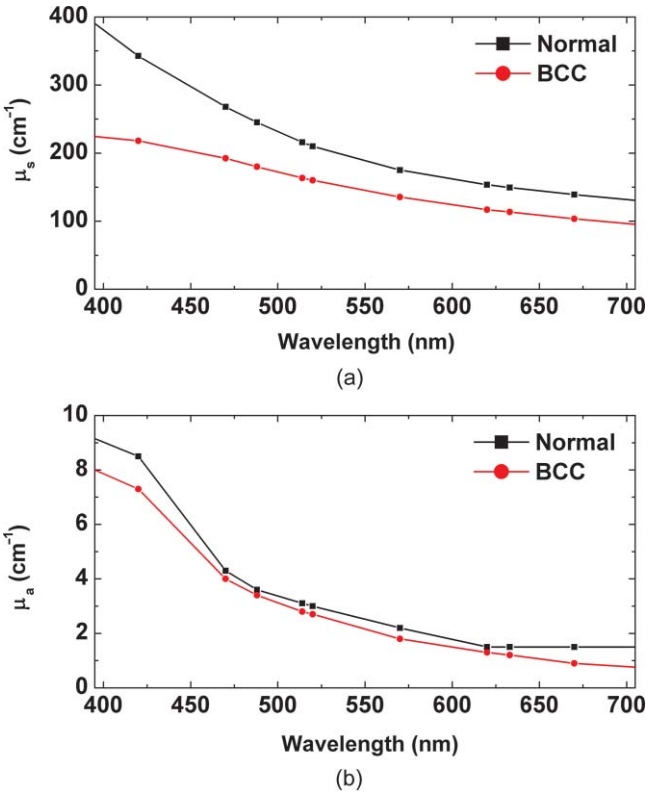


**Fig. 2** Spectral characteristics and model inputs of (a) normal skin and basal cell carcinoma scattering coefficients and (b) normal skin and basal cell carcinoma absorption coefficients. Data from Salomatina et al. (Ref. 30).

A stock solution of PpIX in dimethylsulfoxide was produced with a concentration of 45 $\mu$g/ml. The solution was then placed in a cuvette, where a spectrophotometer (Hitachi Spectrophotometer U-3010) was used to measure the optical absorbance and the absorption coefficient for PpIX was determined to be 0.06 cm$^{-1}$ at 630 nm, using an extinction coefficient for PpIX, $\varepsilon_{630\,\mathrm{nm}} = 0.0014\ \mu\mathrm{g/ml}^{-1}\ \mathrm{cm}^{-1}$. This is within the range of values published in the literature.[10]

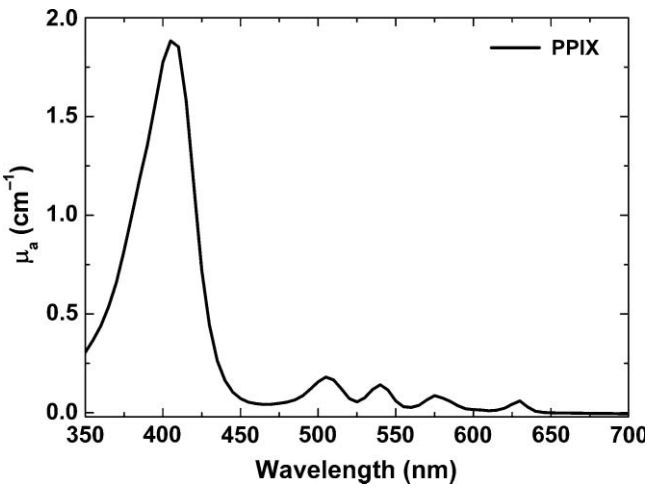


**Fig. 3** Absorption coefficient for PpIX as a function of wavelength.

For the PDT treatment simulations, we based the inputs for our model on the well-established treatment parameters used in the Scottish Photodynamic Therapy Centre, Ninewells Hospital & Medical School, Dundee. The entire top surface of the cube was irradiated uniformly, at the treatment wavelength of 632 nm. A surface irradiance, $\Psi_0$, of 82 mW/cm$^2$ was delivered over a simulated treatment time of ~30 min, thus administrating a simulated total treatment LD of 150 J/cm$^2$. The photons propagated through the normal skin and tumor using the scattering and absorption coefficient values at this wavelength. After photon absorption in the tissue, the amount of energy deposited was calculated. The energy absorbed in the tumor was determined at each time step, corresponding to increments of 40 s. On the basis of our assumptions of the PD, it was possible to infer the 3-D distribution of photons and, hence, 3-D distribution of singlet oxygen production in the tumor as a function of LD.

For the PDT fluorescence simulations, PpIX fluorescence photons were induced at specific stages during the PDT treatment simulations. The entire top surface of the cube and cylinder was irradiated uniformly at the fluorescence excitation wavelength of 400 nm. Fluorescence photons that exited the top surface were tracked from their place of origin, and it was then possible to know exactly where they came from inside the tumor. After each PDT treatment simulation was carried out, the PDT fluorescence simulation followed immediately afterward. In other words, the two simulations were run simultaneously for given time steps (i.e., every 40 to ~1800 s). In this manner, PpIX fluorescence was detected in the tumor as a function of depth and LD in the presence of photobleaching.

## 3 Results

### 3.1 *In vivo 5-Aminolaevulinic Acid–Induced Protoporphyrin IX Fluorescence Spectra*

Figure 4 illustrates the mean fluorescence of the eight spectra from each of the six patients before the application of the 5-ALA cream. Figure 5 presents PpIX fluorescence spectra noninvasively measured in six different patients as a function of time during treatment. Note that in both sets of figures, the overall mean of all six patients is highlighted by a thick solid line. As depicted by Fig. 4(a), collected peak autofluorescence signals of ~500 nm are highly variable between patients. Collected PpIX fluorescence signals of ~635 nm can also vary between patients, as illustrated in Fig. 4(b). Figure 5 illustrates that, after topical application of 5-ALA, there is a wide variability seen in the collected PpIX fluorescence signals among the six patients examined at each time point of treatment. Each baseline fluorescence spectrum measurement was subtracted from their corresponding fluorescence spectrum measurement at the three different time points of treatment (i.e., before, halfway through and after treatment).

### 3.2 *Photobleaching Observed during Clinical Photodynamic Therapy*

*In vivo* photobleaching was monitored through the use of the clinical patient sBCC fluorescence data collected and discussed above. Figure 6(a) depicts the mean PpIX fluorescence intensity from the six patients at the time points of treatment. As

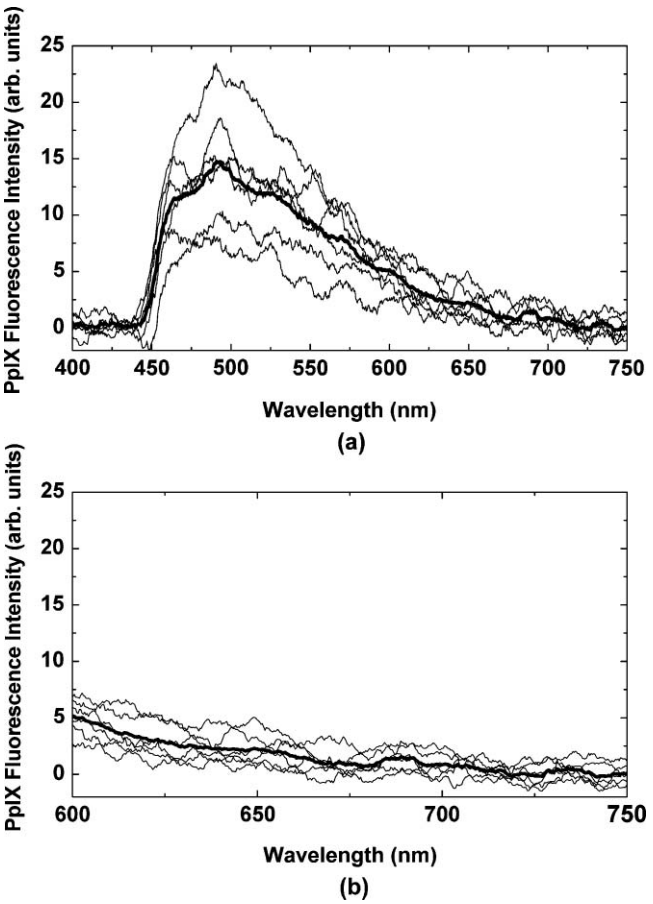


**Fig. 4** Baseline fluorescence spectra recorded before 5-ALA application for six patients; the mean is depicted in bold. (a) Spectral region showing tissue autofluorescence and (b) spectral region where PpIX fluorescence peak will feature.

expected, this decreases from the outset to the end of treatment and illustrates how the peak PpIX fluorescence reduces as treatment progresses and photobleaching occurs. For each patient, the PpIX fluorescence intensity values recorded at ~635 nm were normalized to each of their individual maximum PpIX fluorescence intensity value. Each point, therefore, in Fig. 6(b) represents normalized PpIX fluorescence intensity values recorded at ~635 nm from patients at particular time points during their respective treatment times. Assuming photobleaching follows a single exponential decay curve, a time constant, $\tau$, of 172 s represents the best fit to the data presented in Fig. 6(b). The photobleaching dose constant, $\beta$, was then calculated according to Eq. (5). At a mean surface irradiance, ($\Psi_0$), of 82 mW/cm$^2$, a mean value of $\beta = 14$ J/cm$^2$ with an associated standard deviation of 1 J/cm$^2$ was obtained.

$$\beta = \tau(\Psi_0). \tag{5}$$

In the literature, a range of values of $\beta$ has been provided (1.8–33 J/cm$^2$) in various studies.[9,10,27,33] Such a wide variation in the value of $\beta$ may arise from a range of factors, including the time between administration of the drug to treatment beginning, the fluence rate used for illumination, the type of animal system investigated, and the type of tumor being treated. In our case, this value was derived from clinically obtained data for human patients presenting with sBCC.

### 3.3 *Monte Carlo Predictions of Protoporphyrin IX Fluorescence Originating in a Tumor*

As illustrated in Fig. 7(a), PpIX fluorescence photons generated at deeper tumor depths have a lower probability of escape from the tumor than PpIX fluorescence photons generated at shallower tumor depths. When the treatment simulation progressed and photobleaching increased, the PpIX fluorescence emitted from the surface of the tumor decreased and more PpIX fluorescence that originated from deeper within the tumor was observed at the surface. Initially, fluorescence detected at the surface decreased rapidly with depth. As treatment progressed, the fluorescence detected from photons near the surface decreased. From halfway through treatment (75 J/cm$^2$), almost all surface fluorescence was derived from photons deep within the tumor. The output power of PpIX fluorescence detected at the tumor surface at LD = 0 J/cm$^2$, was denoted as ${}^{P}F_{t=0} = 6.8 \times 10^{-5}$ W. The total fraction of PpIX fluorescence detected at the tumor surface at LD = 37.5, 75, 112.5, and 150 J/cm$^2$ compared to ${}^{P}F_{t=0}$ was $1.95 \times 10^{-3}$, $1.2 \times 10^{-4}$, $2.77 \times 10^{-5}$, and $3 \times 10^{-6}$, respectively. Figure 7(b) illustrates the effect of increasing LD and photobleaching in the treatment simulation demonstrating a reduction in the total PpIX fluorescence detected at the tumor surface. There is a difference of almost six orders of magnitude in the PpIX fluorescence detected from the surface of the tumor between LD = 0 J/cm$^2$ ($t = 0$ s) and LD = 150 J/cm$^2$ ($\sim t = 1800$ s). A decrease of approximately three orders of magnitude is evident between 0 and 37.5 J/cm$^2$, indicating a large decrease in PpIX fluorescence pertaining to rapid photobleaching followed by a slower photobleaching thereafter.

In order to compare our model, which used clinical data reported in the present paper, to clinical data reported by Cottrell et al.,[34] results were reanalyzed using excitation and emission wavelengths of 632 and 705 nm, respectively [Fig. 8(a)]. Our simulated normalized PpIX fluorescence curve—which corresponds to 82 mW/cm$^2$—was compared to two other fluence rates, namely, 150 and 60 mW/cm$^2$, taken from the clinical data for sBCC reported by Cottrell et al.[34] In the MC model, we used our clinically determined photobleaching dose constant, $\beta$, of 14 J/cm$^2$ and found that our simulated PpIX fluorescence data were in close agreement with the clinical data of Cottrell et al.[34] up to a fluence of ~8 J/cm$^2$. Our simulated normalized PpIX fluorescence signal then decreased below the clinical normalized PpIX fluorescence signal corresponding to 60 mW/cm$^2$.

Figure 8(b) is an extension of Fig. 8(a) and illustrates how the normalized PpIX fluorescence continues to decrease up to 150 J/cm$^2$. At this point we found that a small quantity of PpIX fluorescence was still evident in the tumor. The data in both these graphs use the logarithmic $y$-axis to display the normalized PpIX fluorescence more clearly. Interestingly, Cottrell et al.[34] illustrated that PpIX fluorescence was still present up to a fluence of 200 J/cm$^2$, when treated with 150 mW/cm$^2$, suggesting that photobleaching may still be occurring.

### 3.4 *Monte Carlo Simulations of Singlet Oxygen Produced in a Tumor*

In addition to the PpIX fluorescence detected, singlet oxygen produced at depths in the tumor was also modeled at each time step. At LD = 0 J/cm$^2$ ($t = 0$ s)—in other words, before

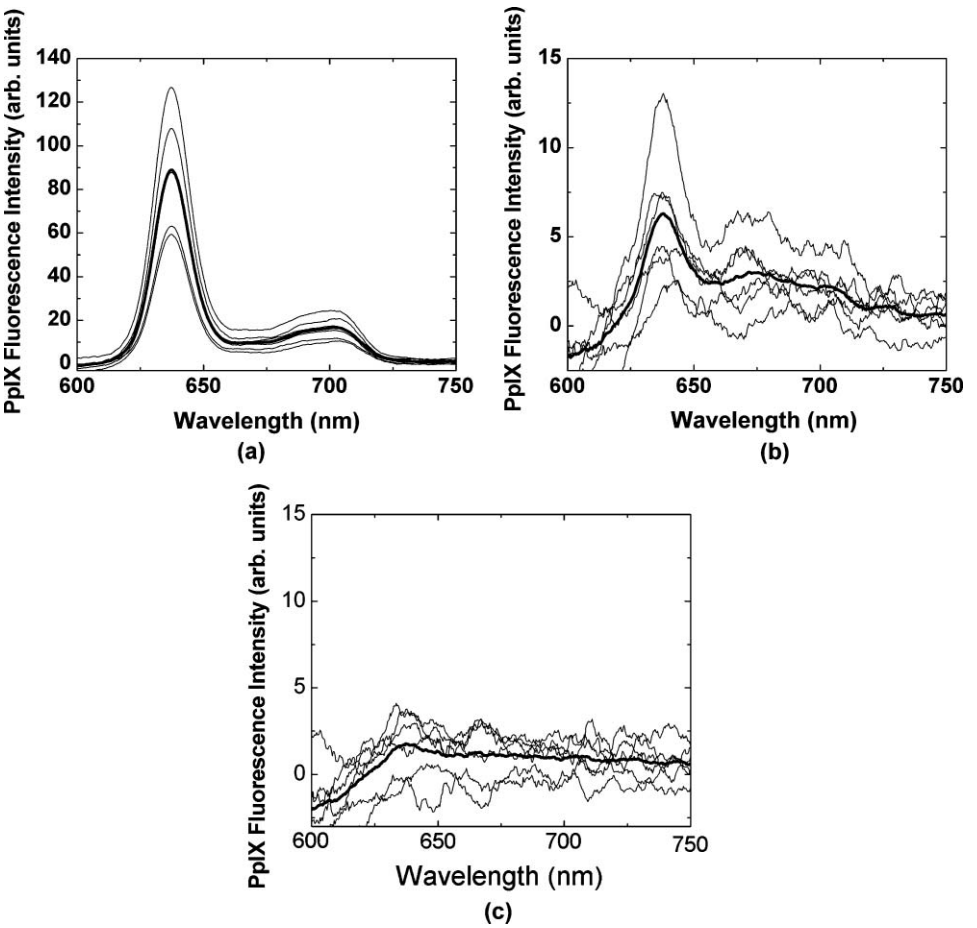


**Fig. 5** PpIX fluorescence spectra recorded for six patientsl the mean is depicted in bold. (a) immediately prior to treatment, (b) halfway through treatment, and (c) immediately after PDT treatment.

photobleaching—a large quantity of singlet oxygen was evident, particularly at the surface of the tumor. As treatment progressed, the superficial layers of the tumor became photobleached and less singlet oxygen was produced in these layers. When the treatment continued further, a larger quantity of singlet oxygen could be seen to be produced deeper within the tumor than at the surface. This became more apparent during the latter stages of the treatment simulation. The majority of the PD occurs early on in PDT treatments and reduces as the treatment progresses. However, there is still a small but potentially useful quantity of singlet oxygen produced with an increasing LD in deeper layers of the tumor as shown in Table 1. This singlet oxygen produced is expressed as a fraction of the maximum singlet oxygen produced at the surface of the tumor, $z = 0$, and at the treatment light dose, LD $= 0$ J/cm$^2$, denoted as, ${}^{S}O_{LD=0,z=0}$ and equal to $5.79 \times 10^{17}$ photons/cm$^3$.

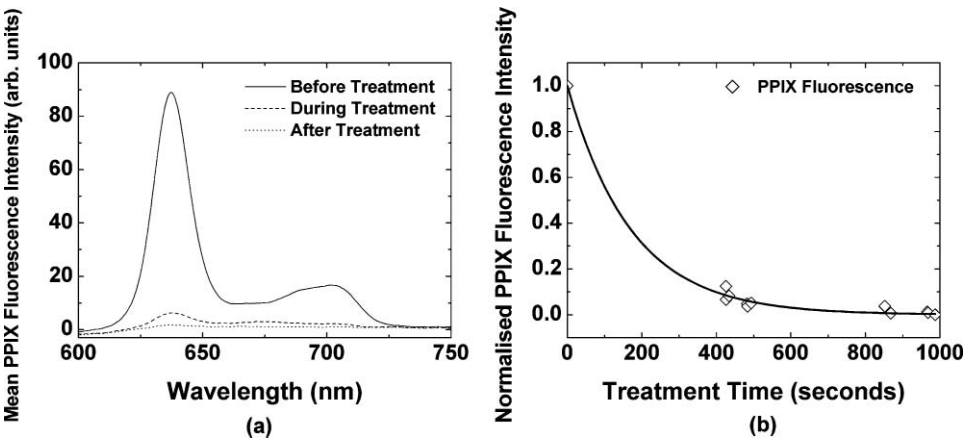


**Fig. 6** (a) Mean PpIX Fluorescence Intensity (peak points ~635 nm) recorded from six sBCC before, halfway during and after clinical PDT treatments, and (b) mean normalized PpIX fluorescence intensity (peak points ~635 nm) of six sBCC before, halfway during and after PDT treatment.

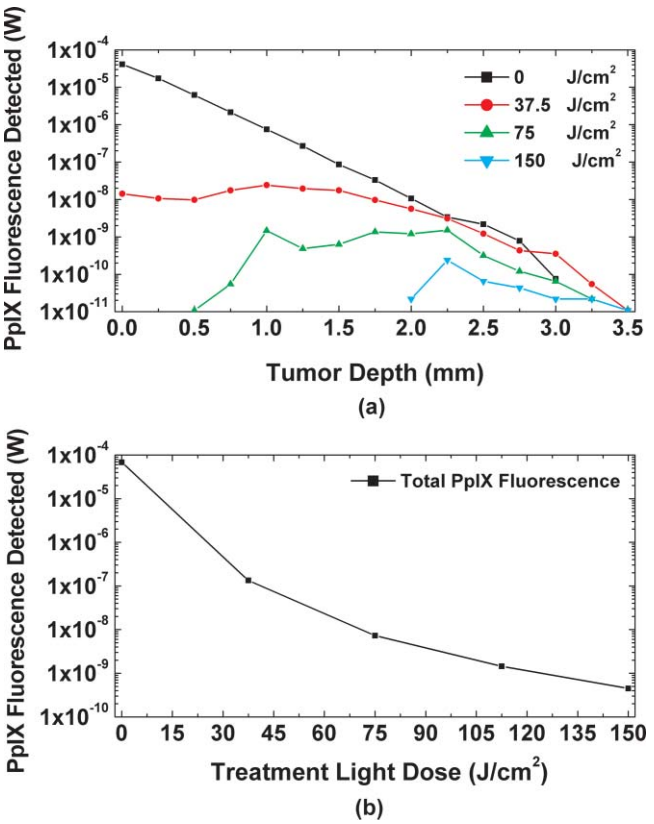


**Fig. 7** (a) PpIX fluorescence detected at the surface that has originated from varying depths in the tumor with increasing LD in the treatment and fluorescence simulations and (b) total PpIX fluorescence detected at the surface of the tumor with increasing LD in the treatment and fluorescence simulations.

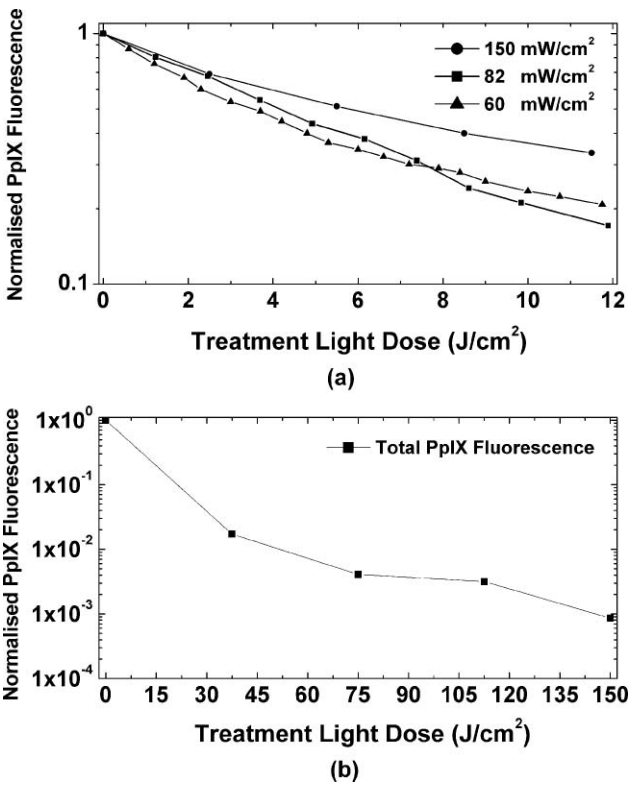


**Fig. 8** (a) Comparison of normalized PpIX fluorescence (705 nm) detected at the surface of the tumor as a function of treatment light dose from our model using 82 mW/cm$^2$ to clinical data reported by Cottrell et al.[34] at 60 and 150 mW/cm$^2$. (b) Total normalized PpIX fluorescence (705 nm) detected at the surface of the tumor with increasing LD in the treatment and fluorescence simulations.

The singlet oxygen produced at all time points of the treatment simulation was then added together to obtain the singlet oxygen produced in a tumor over the entire treatment simulation as a function of tumor depth and LD. This is shown in Fig. 9(a). The horizontal line indicates the necrosis threshold photodynamic dose, $PD_T$, assumed to be $8.6 \times 10^{17}$ photons/cm$^3$ absorbed by the photosensitizer per unit volume of tissue.[30] Therefore, we found that the maximum depth achieved of singlet oxygen produced in the tumor after administrating a total treatment LD of 37.5, 75, 112.5, and 150 J/cm$^2$ was 2.0, 2.7, 3.0, and 3.3 mm, respectively. This is illustrated in Fig. 9(b). PDT with red light is an effective treatment for nonmelanoma skin cancers with a thickness of 1–3 mm. The results here are in good agreement with those quoted in the literature.[4,35]

## 3.5 *Effects of Optical Properties*

The results presented in Figs. 7–9 are based on optical properties described by Salomatina et al.,[30] derived from nonmelanoma human skin cancer *in vitro*. These optical

**Table 1** Singlet oxygen produced at varying depths in the tumor at specific time points in the treatment simulation as a fraction of the maximum singlet oxygen produced at the tumor surface. ($^SO_{LD=0,z=0} = 5.79 \times 10^{17}$ photons/cm$^3$).

| | $^SO_{LD,z}$ / $^SO_{LD=0,z=0}$ | | | |
|---|---|---|---|---|
| Tumor depth | Treatment LD (J/cm$^2$) | | | |
| (mm) | 37.5 | 75 | 112.5 | 150 |
| 1 | $1.1 \times 10^{-2}$ | $2.0 \times 10^{-4}$ | $3.0 \times 10^{-6}$ | $6.3 \times 10^{-8}$ |
| 2 | $5.5 \times 10^{-2}$ | $1.3 \times 10^{-2}$ | $2.7 \times 10^{-3}$ | $6.4 \times 10^{-4}$ |
| 3 | $5.0 \times 10^{-2}$ | $3.0 \times 10^{-2}$ | $1.6 \times 10^{-2}$ | $9.4 \times 10^{-3}$ |
| 4 | $3.1 \times 10^{-2}$ | $2.5 \times 10^{-2}$ | $1.8 \times 10^{-2}$ | $1.4 \times 10^{-2}$ |

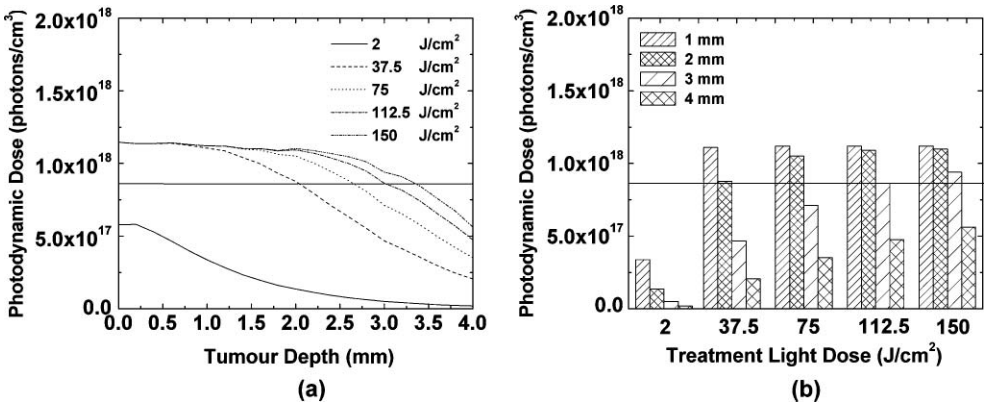


**Fig. 9** Singlet oxygen production in units of photons/cm$^3$ absorbed by the photosensitizer in the tumor (a) as a function of depth and LD, and (b) maximum depth achieved after a given time. The threshold photodynamic dose, $PD_T$, assumed to be $8.6 \times 10^{17}$ photons/cm$^3$ absorbed by the photosensitizer is signified by a horizontal line.

properties appear to be well suited for the present study and thus were incorporated in the MC model. Further simulations were performed to investigate how the collected PpIX fluorescence signal and the generated singlet oxygen changed with different optical properties. These optical properties—used to represent tumor optical properties—were derived from human skin tissue *in vitro*, sourced from two independent studies and cover a wide spectral range, which is of interest to us.[31,32]

Figures 2(a) and 2(b) depict the curves of the optical properties used to produce Fig. 9. The scattering anisotropy factor, $g$, was taken as 0.8 when using the optical properties derived by Salomatina et al.[30] and 0.9 when using the optical properties derived by both Bashkatov et al.[31] and Chan et al.[32] Bashkatov et al.[31] had the lowest absorption coefficients and highest scattering coefficients as a function of wavelength for the three optical property sets. Furthermore, Chan et al.[32] had the highest absorption coefficients as a function of wavelength. Figure 10(a)

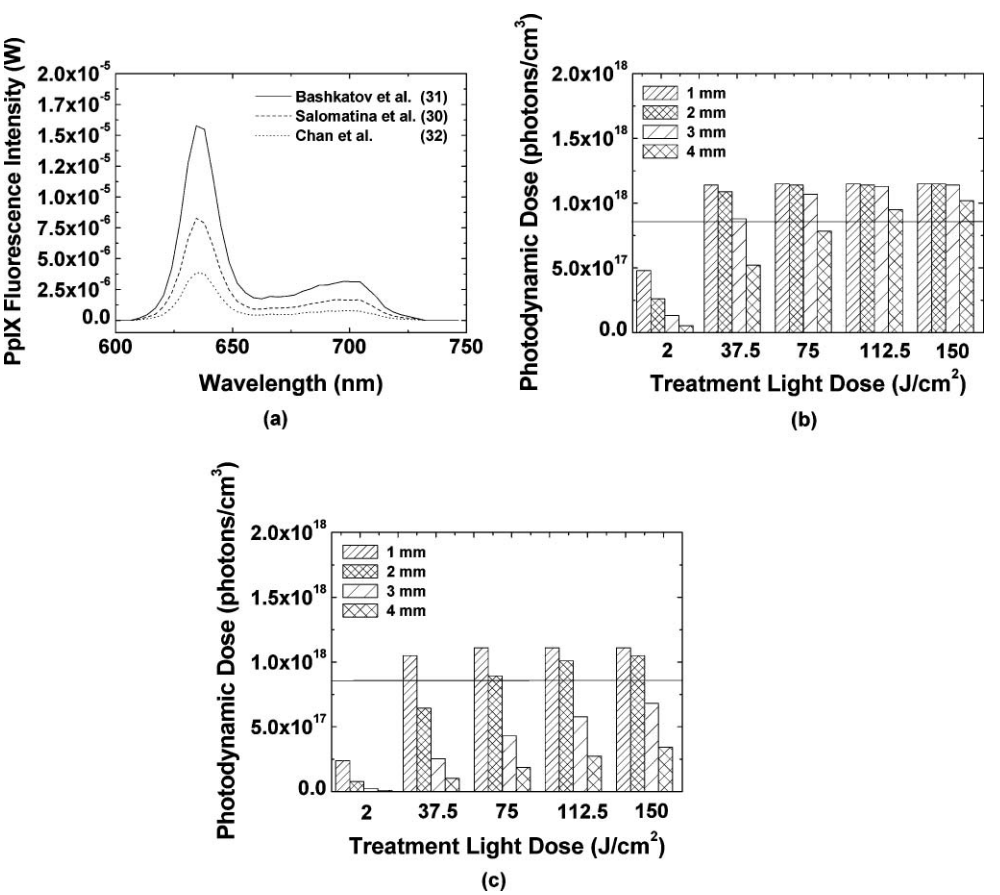


**Fig. 10** (a) illustrates how different sets of optical properties affected the absolute value of the collected PpIX fluorescence signal, (b) represents the effects of optical properties obtained from Bashkatov et al. (Ref. 31) on the singlet oxygen production, and (c) represents the effects of optical properties obtained from Chan et al. (Ref. 32) on the singlet oxygen production.

illustrates how different sets of optical properties affected the absolute value of the collected PpIX fluorescence signal, while Figs. 10(b) and 10(c) represent there effect on the generated singlet oxygen.[31,32] The photobleaching dose constant, $\beta$, was fixed at 14 J/cm$^2$ for all the simulations when considering different sets of optical properties as inputs for the model. In light of this, optical property variations could explain the differences in the empirical PpIX fluorescence spectra recorded from the six patients presented in Fig. 5.

## 4 Discussion

We employed the PDT implicit dosimetry model, which uses fluorescence photobleaching kinetics of a photosensitizer as a dose metric.[6] Noninvasive monitoring of the *in vivo* PpIX fluorescence signal collected during clinical T-PDT enabled the prediction of singlet oxygen generation from which the PD in a tumor can be inferred. The empirical data showed a reduction in the detected PpIX fluorescence that was used as an indicator of *in vivo* PpIX photobleaching. From our clinical results an *in vivo* photobleaching dose constant, $\beta$, of 5-ALA-induced PpIX fluorescence was found to be $14 \pm 1$ J/cm$^2$. We have shown that the majority of the PpIX fluorescence signal has disappeared halfway during treatment, is no longer visible to the naked eye, and is again further reduced albeit to a lesser extent at the end of treatment. Similar clinical findings have been reported by Hewett et al.,[36] where they point out that there was a discernible reduction in PpIX fluorescence after only 100 s (dose = 12 J/cm$^2$). Furthermore, they state that the 630-nm fluorescence was reduced to the surrounding tissue background level by 300 s into the treatment. Ericson et al.[33] reported a high rate of photobleaching up to a cumulative light dose of 10 J/cm$^2$.

Our 3-D MC model provides a qualitative description of both the collected PpIX fluorescence signal and the generated singlet oxygen. MC simulations taking into account photobleaching were performed in an attempt to determine the spatial and temporal changes to the origin of collected PpIX fluorescence and generated singlet oxygen with increasing LD and at varying depths in the tumor. This MC model has been designed to mimic both the clinical situation under investigation and the procedure by which treatment and *in situ* monitoring take place. It is capable of simulating entire PpIX fluorescence spectra and enabled us to examine further clinical observations and investigate the inherent, complex nature of T-PDT. Following a similar route to those present in the literature, a range of assumptions have been made to enable our investigation of the PpIX fluorescence detected and the singlet oxygen generated during a PDT treatment (Sec. 2.4).

During PDT treatment, the photosensitizer near the surface photobleaches and, therefore, the PpIX fluorescence detected at greater depths contributes more to the surface fluorescence signals detected [Fig. 7(a)]. Figure 7(b) illustrates that most of the surface PpIX fluorescence has disminished toward the end of treatment. The total fraction of PpIX fluorescence detected at the tumor surface at LD = 37.5, 75, 112.5, and 150 J/cm$^2$ compared to ${}^{P}F_{t=0}$ was $1.95 \times 10^{-3}$, $1.2 \times 10^{-4}$, $2.77 \times 10^{-5}$, and $3 \times 10^{-6}$, respectively. Nonetheless, a small but potentially useful quantity of singlet oxygen was still being produced at depth within the tumor as shown in Table 1.

A potential limitation to the model is the fact that oxygen concentration is constant, and it is assumed that availability of oxygen does not compromise the effectiveness of treatment. It has been reported that oxygenation may be maintained during light illumination, particularly if low fluence rates are used.[37] However, recent studies have reported that $\beta$ is not constant and is varying both temporally and spatially within the tissue.[34,38] These studies observed fluence rate-dependent photobleaching kinetics that were attributable to oxygen supply to the treated tissue. This is particularly true when using different fluence rates.

We acknowledge from Fig. 8(a) that in order to reproduce the clinical data of Cottrell et al.[34] more accurately, $\beta$ would need to increase with time—essentially slowing the photobleaching rate as a function of time and fluence—which is presumably due to decreased oxygen levels as the treatment progresses. This suggests that $\beta$ may not be constant for a constant fluence rate. However, it is difficult to ascertain how $\beta$ would change after 12 J/cm$^2$.

Therefore, in order to change $\beta$ accurately as a function of fluence, it is necessary to have comprehensive clinical data, with a large sample size of patients, which extends up to at least 150 J/cm$^2$. Moreover, in our model we have sought to represent the situation that pertains within most PDT clinics (i.e., excitation at 405 nm for fluorescence induction and treatment at 632 nm). However, Cottrell et al.[34] used different parameters. More detailed studies of fluorescence and/or oxygen measurements *in vivo* are necessary to ascertain how oxygen changes as a function of fluence during treatment. Tumor oxygenation and the change thereof during PDT with systemically administered Photofrin® has been studied by Henderson et al.[39] However, lack of well-established real-time oxygen measurements recorded *in vivo* during ALA-PDT of sBCC makes it difficult to ascertain how oxygen changes during treatment. Furthermore, the determination of $\beta$ could be further complicated *in vivo* by variations in the vascularization of the tumor, skin temperature, tissue optical properties, and the spatial distribution of the photosensitizer. We have used a constant $\beta$ because this fits the clinical data that were derived in this study. There is certainly a need for more clinical PpIX fluorescence data, such as that published by Cottrell et al.,[34] and our results highlight this. In line with previous work carried out by Farrell et al.[10] we assumed a constant $\beta$, implying that the tumor was fully oxygenated for the duration of the treatment, which had no limiting effects on the production of singlet oxygen.

Data from clinical ALA-PDT treatments reported by our own group in tumor tissue[40] show a similar time course to that reported by Cottrell et al.,[34] namely, a rapid initial photobleaching followed by a slowly decaying fluorescence level as treatments progressed. The slower rate of photobleaching could be due to oxygen, as mentioned above, and/or due to a spatially inhomogeneous PpIX concentration in the tumor, as suggested by Kruijt et al.[41] in rat esophagus.

However, it has been shown that photobleaching *in vivo* can be depth dependent; as the photobleaching at the surface is completed, the fluorescence decays at a slower rate due to detection of fluorescence emission from deeper layers.[29] It has been reported by other groups that ALA penetration depths may range between 2 and 5 mm.[42–44] We have therefore assumed a homogeneous distribution of PpIX in our modeled tumor, with

a thickness of 4 mm, which is within this reported range. We acknowledge that the depth-dependent concentration of PpIX together with delivered fluence is important in PDT dosimetry. It has been reported in the past that increasing the uptake of ALA penetration by deep BCC lesions could be improved by prolonging the topical application time.[45] This could potentially allow for a more homogeneous distribution of PpIX within the tumor. We have sought to investigate the issue of delivered fluence to the tumor. Therefore, we believe that an opportunity exists to optimize PDT regimes for deep BCC by delivering a larger treatment light dose to the tumor.

Monitoring the change in the surface photosensitizer fluorescence signals during PDT due to photobleaching may be used to predict the depth of necrosis.[10,46] The $PD_T$ is illustrated in Fig. 9 by the horizontal lines. Therefore, the depth of necrosis based on the generation of singlet oxygen in the tumor was found to be 2.0, 2.7, 3.0, and 3.3 mm after an administered LD of 37.5, 75, 112.5, and 150 J/cm$^2$ [Fig. 9(b)], for an adopted specific set of optical properties. To the best of our knowledge, the optical properties we have used in Fig. 9 are the most comprehensive to date representing nonmelanoma skin cancers. These results suggest that an increase from our typical administered treatment light dose of 75–150 J/cm$^2$ could increase the effective PDT treatment initially achieved at a depth of 2.7–3.3 mm in the tumor, respectively. Furthermore, this increase reduced the surface PpIX fluorescence from $1.2 \times 10^{-4}$ to $3 \times 10^{-6}$ of ${}^{P}F_{t=0}$. Oseroff et al.[47] previously suggested the need for a treatment light dose of at least 100 J/cm$^2$ at 635 nm.

It is well known that the effect of tissue optical properties can affect the collected fluorescence signal.[15] Therefore, we need to be cautious in our interpretation of the empirical fluorescence data. Optical property effects may be responsible for the observed variations in the collected PpIX fluorescence signals between the patients presented in Fig. 5. Correct interpretation of the photobleaching data (Fig. 6.) requires that the empirical PpIX fluorescence data have been corrected for changes in optical properties. MC simulations were performed using a range of optical properties from the literature. The results presented in Fig. 10 indicate that changing the optical properties affected the absolute value of the collected PpIX fluorescence signal and the generated singlet oxygen. This, in turn, impacted on the penetration of light and, hence, the PD administered to the tumor. However, the recommendation of administrating a larger light dose, which advocates an increase in the treatment time after surface PpIX fluorescence has diminished, remained valid for different sets of optical properties and therefore should have a beneficial outcome on the total treatment effect.

This MC model can be considered as a reasonable approach to establishing tailored optimal treatment regimes for clinical T-PDT based on *in vivo* PpIX fluorescence measurements recorded from patients presenting with sBCC. We have demonstrated a relationship between surface PpIX fluorescence and the PD at varying depths in a tumor and at different LD administered during a simulated PDT treatment, in the presence of photobleaching. In light of the results presented in this paper, we suggest that an increase in the treatment light dose beyond the disappearance of surface PpIX fluorescence may continue to provide effective PDT treatment at depth within tumors. This increase in the time of light administration may ultimately assist in optimizing PDT treatment regimes. If patients were treated for longer, this could potentially eliminate remnants of the lesion deeper down in the skin tissue, eradicating residual disease and reducing recurrance rates. Administrating a larger treatment light dose means increasing the treatment time, and this may have a negative impact on patients, particularly those who experience severe pain during treatment. Pain can be a limiting factor to successful PDT.[48] However, it has been shown that PDT pain is higher, initially, and decreases during treatment.[33] Failure to deliver effective PDT treatments impacts the welfare of patients and their quality of life. Follow-up in PDT clinics are critically important, and decisions are facilitated pending the outcome of these assessments. Ultimately, if longer treatment times were advocated, it may be possible to achieve highly successful long-term clinical outcomes, while saving time, money, and hospital resources.

## Acknowledgments

This work was supported by the Barbara Stewart Charitable Trust, Scottish PDT Centre at Ninewells Hospital & Medical School, Dundee, and the School of Physics and Astronomy, University of St. Andrews, St. Andrews, Scotland, United Kingdom.

## References

1. T. J. Dougherty, "Photodynamic therapy," *Photochem Photobiol.* **58**, 895–900 (1993).
2. S. Nonell and R. W. Redmond, "On the determination of quantum yields for singlet molecular oxygen photosensitization," *J. Photochem. Photobiol. B* **22**, 171–172 (1994).
3. K. R. Weishaupt, C. J. Gomer, and T. J. Dougherty, "Identification of singlet oxygen as the cytotoxic agent in photo-inactivation of a murine tumor," *Cancer Res.* **36**, 2326–2329 (1976).
4. C. A. Morton, K. E. McKenna, and L. E. Rhodes, "Guidelines for topical photodynamic therapy: update," *Br. J. Dermatol.* **159**, 1245–1266 (2008).
5. F. W. Hetzel, S. M. Brahmavar, Q. Chen, S. L. Jacques, M. S. Patterson, B. C. Wilson, and T. C. Zhu, "Photodynamic therapy dosimetry," AAPM Report No. 88, Am. Assn. of Physicists in Medicine, Medical Physics Publishing (July 2005).
6. B. C. Wilson, M. S. Patterson, and L. Lilge, "Implicit and explicit dosimetry in photodynamic therapy: a new paradigm," *Lasers. Med. Sci.* **12**, 182–199 (1997).
7. T. S. Mang, T. J. Dougherty, W. R. Potter, D. G. Boyle, S. Somer, and J. Moan, "Photobleaching of porphyrins used in photodynamic therapy and implications for therapy," *Photochem. Photobiol.* **45**, 501–506 (1987).
8. I. Georgakoudi and T. H. Foster, "Singlet oxygen- versus nonsinglet oxygen-mediated mechanisms of sensitizer photobleaching and their effects on photodynamic dosimetry," *Photochem. Photobiol.* **67**(6), 612–625 (1998).
9. D. J. Robinson, H. S. de Bruijn, N. Van Der Veen, M. R. Stringer, S. B. Brown, and W. M. Star, "Fluorescence photobleaching of ALA-induced protoporphyrin IX during photodynamic therapy of normal hairless mouse skin: the effect of light dose and irradiance and the resulting biological effect," *Photochem. Photobiol.* **67**(1), 140–149 (1998).
10. T. J. Farrell, R. P. Hawkes, M. S. Patterson, and B. C. Wilson, "Modeling of photosensitiser fluorescence emission and photobleaching for photodynamic therapy dosimetry," *Appl. Opt.* **37**(31), 7168–7183 (1998).
11. S. K. Chang, N. Marin, M. Follen, and R. Richards-Kortum, "Model-based analysis of clinical fluorescence spectroscopy for *in vivo* detection of cervical intraepithelial dysplasia," *J. Biomed. Opt.* **11**(2), 024008 (2006).
12. E. Drakaki, M. Makropoulou, and A. A. Serafetinides, "*In vitro* fluorescence measurements and Monte Carlo simulation of laser irradiation propagation in porcine skin tissue," *Lasers Med. Sci.* **23**, 267–276 (2008).

13. G. Yoon, A. J. Welch, M. Motamedi, and M. C. J. van Gemert, "Development and application of three-dimensional light distribution model for laser irradiated tissue," *IEEE J. Quantum Electron.* **QE-23**, 1721–1733 (1987).
14. M. Keijzer, W. M. Star, and P. R. M. Storchi, "Optical diffusion in layered media," *Appl. Optics.* **27**, 1820–1824 (1988).
15. J. Swartling, A. Pifferi, A. M. K. Enejder, and S. Andersson-Engels, "Accelerated Monte Carlo models to simulate fluorescence spectra from layered tissues," *J. Opt. Soc. Am. A.* **20**(4), 714–727 (2003).
16. M. Keijzer, S. L. Jacques, S. A. Prahl, and A. J. Welch, "Light distributions in artery tissue: Monte Carlo simulations for finite-diameter laser beams," *Lasers Surg. Med.* **9**, 148–154 (1989).
17. H. Moseley, "Light distribution and calibration of commercial PDT LED arrays," *Photochem. Photobiol. Sci.* **4**, 911–914 (2005).
18. V. Nadeau, M. O'Dwyer, K. Hamdan, I. Tait, and M. Padgett, "*In vivo* measurement of 5-aminolaevulinic acid-induced protoporphyrin IX photobleaching: a comparison of red and blue light of various intensities," *Photodermatol. Photoimmunol. Photomed.* **20**, 170–174 (2004).
19. L. Wang, S. L. Jacques, and L. Zheng, "MCML—Monte Carlo modeling of light transport in multi-layered tissues," *Comput. Methods Programs Biomed.* **47**, 131–146 (1995).
20. A. J. Welch, C. Gardner, R. Richards-Kortum, E. Chan, G. Criswell, J. Pfefer, and S. Warren, "Propagation of Fluorescent Light," *Lasers Surg. Med.* **21**, 166–178 (1997).
21. M. L. de Jode, "Monte Carlo simulations of light distributions in an embedded tumour model: studies of selectivity in photodynamic therapy," *Lasers Med. Sci.* **15**, 49–56 (2000).
22. L. V. Wang, R. E. Nordquist, and W. R. Chen, "Optimal beam size for light delivery to absorption-enhanced tumors buried in biological tissues and effect of multiple-beam delivery: a Monte Carlo study," *Appl. Opt.* **36**(31), 8286–8291 (1997).
23. L. G. Henyey and J. L. Greenstein, "Diffuse radiation in the galaxy," *Anales d'Astrophysique* **3**, 117–137 (1940).
24. K. Wood, J. E. Bjorkman, B. Whitney, and A. D. Code, "The effect of multiple scattering on the polarization from axisymmetric circumstellar envelopes. I. pure thomson scattering envelopes," *The Astrophysical Journal* **461**, 828–846 (1996).
25. K. Wood, J. E. Bjorkman, B. Whitney, and A. D. Code, "The effect of multiple scattering on the polarization from axisymmetric circumstellar envelopes. II. Thomson scattering in the presence of absorptive opacity sources," *The Astrophysical Journal* **461**, 847–857 (1996).
26. K. Wood and R. J. Reynolds, "A model for the scattered light contribution and polarization of the diffuse H$\alpha$ galactic background," *The Astrophysical Journal* **525**, 799–807 (1999).
27. A. J. L. Jongen and H. J. C. M Sterenborg, "Mathematical description of photobleaching *in vivo* describing the influence of tissue optics on measured fluorescence signals," *Phys. Med. Biol.* **42**, 1701–1716 (1997).
28. M. S. Patterson, B. C. Wilson, and R. Graff, "*In vivo* tests of the concept of photodynamic threshold dose in normal rat liver photosensitized by aluminium chlorosulphonated phthalocyanine," *Photochem. Photobiol.* **51**, 343–349 (1990).
29. S. L. Jacques, R. Joseph, and G. Gofstein, "How photobleaching affects dosimetry and fluorescence monitoring of PDT in turbid media," *Proc. SPIE* **1881**, 168–179 (1993).
30. E. Salomatina, B. Jiang, J. Novak, and A. N. Yaroslavsky, "Optical properties of normal and cancerous human skin in the visible and near-infrared spectral range," *J. Biomed. Opt.* **11**(6), 064026 (2006).
31. A. N. Bashkatov, E. A. Genina, V. I. Kochubey, and V. V. Tuchin, "Optical properties of human skin, subcutaneous and mucous tissues in the wavelength range from 400 to 2000 nm," *J. Phys. D* **38**, 2543–2555 (2005).
32. E. K. Chan, B. Sorg, D. Protsenko, M. O'Neil, M. Motamedi, and A. J. Welch, "Effects of compression on soft tissue optical properties," *IEEE J. Quantum Electron* **4**(2), 943–950 (1996).
33. M. B. Ericson, C. Sandberg, B. Stenquist, F. Gudmundson, M. Karlsson, A.-M. Ros, A. Rosen, O. Larko, A.-M. Wennberg, and I. Rosdahl, "Photodynamic therapy of actinic keratosis at varying fluence rates: assessment of photobleaching, pain and primary clinical outcome," *Br. J. Dermatol.* **151**, 1204–1212 (2004).
34. W. J. Cottrell, A. D. Paquette, K. R. Keymel, T. H. Foster, and A. R. Oseroff, "Irradiance-dependent photobleaching and pain in $\delta$-aminolevulinic acid-photodynamic therapy of superficial basal cell carcinomas," *Clin. Cancer Res.* **14**(14), 4475–4483 (2008).
35. R.-M. Szeimies, C. A. Morton, A. Sidoroff, and L. R. Braathen, "Photodynamic therapy for non-melanoma skin cancer," *Acta Derm. Venereol.* **85**, 483–490 (2005).
36. J. Hewitt, V. Nadeau, J. Ferguson, H. Moseley, S. Ibbotson, J. W. Allen, W. Sibbett, and M. Padgett, "The application of a compact multispectral imaging system with integrated excitation source to *in vivo* monitoring of fluorescence during topical photodynamic therapy of superficial skin cancers," *Photochem. Photobiol.* **73**(3), 278–282 (2001).
37. J. H. Woodhams, A. J. MacRobert, and S. G. Bown, "The role of oxygen monitoring during photodynamic therapy and its potential for treatment dosimetry," *Photochem. Photobiol. Sci.* **6**, 1246–1256 (2007).
38. K. K. Wang, W. J. Cottrell, S. Mitra, A. R. Oseroff, and T. H. Foster, "Simulations of measured photobleaching kinetics in human basal cell carcinomas suggest blood flow reductions during ALA-PDT," *Lasers Surg. Med.* **41**, 686–696 (2009).
39. B. W. Henderson, T. M. Busch, L. A. Vaughan, N. P. Frawley, D. Babich, T. A. Sosa, J. D. Zollo, A. S. Dee, M. T. Cooper, D. A. Bellnier, W. R. Greco, and A. R. Oseroff, "Photofrin photodynamic therapy can significantly deplete or preserve oxygenation in human basal cell carcinomas during treatment, depending on fluence rate," *Cancer Res.* **60**, 525–529 (2000).
40. R. M. Valentine, S. H. Ibbotson, C. T. A. Brown, K. Wood, and H. Moseley, "A quantitative comparison of 5-aminolaevulinic acid- and methyl aminolevulinate-induced fluorescence, photobleaching and pain during photodynamic therapy," *Photochem. Photobiol.* **87**(1), 242–249 (2011).
41. B. Kruijt, H. S. de Bruijn, A. Van Der Ploeg-van den Heuvel, R. W. F. de Bruin, H. J. C. M. Sterenborg, A. Amelink, and D. J. Robinson, "Monitoring ALA-induced PpIX photodynamic therapy in the rat esophagus using fluorescence and reflectance spectroscopy," *Photochem. Photobiol.* **84**, 1515–1527 (2008).
42. Q. Peng, A. M. Soler, T. Warloe, J. M. Nesland, and K. E. Giercksky, "Selective distribution of porphyrins in skin thick basal cell carcinoma after topical application of methyl 5-aminolevulinate," *J. Photochem. Photobiol. B.* **62**(3), 140–145 (2001).
43. L. O. Svaasand, P. Wyss, M. T. Wyss, Y. Tadir, B. J. Tromberg, and M. W. Berns, "Dosimetry model for photodynamic therapy with topically administered photosensitizers," *Lasers Surg. Med.* **18**, 139–149 (1996).
44. A. Johansson, T. Johansson, M. S. Thompson, N. Bendsoe, K. Svanberg, S. Svanberg, and S. Andersson-Engels, "*In vivo* measurement of parameters of dosimetric importance during interstitial photodynamic therapy of thick skin tumors," *J. Bio. Opt.* **11**(3), 034029 (2006).
45. Q. Peng, T. Warloe, J. Moan, H. Heyerdahl, H. B. Steen, J. M. Nesland and K.-E. Giercksky, "Distribution of 5-aminolevulinic acid-induced porphyrins in noduloulcerative basal cell carcinoma," *Photochem. Photobiol.* **62**, 906–913 (1995).
46. J. D. Vollet-Filho, P. F. C. Menezes, L. T. Moriyama, C. Grecco, C. Sibata, R. R. Allison, O. Castro e Silva, and V. S. Bagnato, "Possibility for a full optical determination of photodynamic therapy outcome," *J. Appl. Phys.* **105**, 2038–1–2038–7 (2009).
47. A. R. Oseroff, S. Shieh, N. P. Frawley, R. Cheney, L. E. Blumenson, E. K. Pivnick, and D. A. Bellnier, "Treatment of diffuse basal cell carcinomas and basaloid follicular hamartomas in nevoid basal cell carcinoma syndrome by wide-area 5-aminolevulinic acid photodynamic therapy," *Arch. Dermatol.* **141**, 60–67 (2005).
48. S. Grapengiesser, F. Gudmundsson, O. Larko, M. Ericson, A. Rosen, and A.-M. Wennberg, "Pain caused by photodynamic therapy of skin cancer," *Clin. Exp. Dermatol.* **27**, 493–497 (2002).